A stochastic 3D model for three-phase heterogeneous microstructures in SOFC-electrodes

Léo Théodon, Jérôme Laurencin, Peter Cloetens, Johan Debayle

▶ To cite this version:

HAL Id: emse-03714559

https://hal-emse.ccsd.cnrs.fr/emse-03714559

Submitted on 5 Jul 2022

A STOCHASTIC 3D MODEL FOR THREE-PHASE HETEROGENEOUS MICROSTRUCTURES IN SOFC-ELECTRODES

Léo Théodon
MINES Saint-Etienne
CNRS, UMR 5307 LGF
Centre SPIN
Saint-Etienne, France
l.theodon@emse.fr

Jérôme Laurencin
Université-Grenoble Alpes,
CEA/LITEN
Grenoble, France
jerome.laurencin@cea.fr

Peter Cloetens
European Synchrotron Radiation Facility
Grenoble, France
cloetens@esrf.eu

Johan Debayle
MINES Saint-Etienne
CNRS, UMR 5307 LGF
Centre SPIN
Saint-Etienne, France
debayle@emse.fr

ABSTRACT

An original stochastic model to simulate complex 3D microstructures of SOFC-electrodes with gradient and global heterogeneity has been developed. The synthetic microstructures generated by the model were compared to real microstructures of Ni-YSZ electrodes acquired by tomography. The ability of the model to generate representative microstructures has been demonstrated. Finally, the model was fitted on real electrode reconstructions. The results obtained shown that the phase surface area density curves and several microstructural properties of the synthetic microstructures were very close to those of the real ones. The flexibility of the model and the results obtained shown that it could be used in the framework of numerical microstructural optimizations of SOFC-electrodes.

Keywords 3D microstructure model · Image analysis · Simulation · Solid oxide fuel cell · Stochastic geometry

1 Introduction

The modeling of three-phase microstructures using stochastic geometry techniques is a major challenge in the context of developing digital twins for solid oxide fuel cell (SOFC) electrodes. The control of the microstructure properties and its optimization is crucial in order to improve the cell performance in operation [1]. Moreover, the agglomeration of the nickel phase, as well as its redistribution in the electrode after several hours of use have a significant impact on the cell life time [2][3].

In this context, many stochastic models have been developed to reflect the geometrical properties of three-phase microstructures. Such models can be based on hard spheres packing [4][5], Gaussian random fields [6][7], or even random graphs [8]. These models are effective in capturing the local heterogeneities in the typical SOFC electrodes with respect to properties such as specific surface area, tortuosity or constrictivity. All these models consider an homogeneous distribution of the phases in the microstructure.

Nevertheless, Fig. 1 and Fig. 2 show that it is necessary to model structures with strong global heterogeneity due to phase gradients and/or the depletion of the metallic phase (Ni) at the interface with the electrolyte. For all these reasons, a model able to take into account this global phase heterogeneity is hereby proposed. The originality of the method comes from the fact that it enables to model SOFC-electrode interfaces using stochastic geometry tools.

In the following section, the characteristics of the proposed model are defined and examples of realizations are presented. Then, the optimization process is described, followed by the validation step and the obtained results. Finally, a conclusion summarizes the approach and opens new perspectives.

2 3D microstructures reconstruction and characterization

2.1 Image reconstruction

In the present study, the electrodes active layers of both cells are reconstructed by synchrotron X-ray holotomography [9] [10]. This method has the advantage of being able to represent 3D volumes with a large field of view (50 μm) and to capture details of the order of a tenth of a nanometer. The microstructure reconstructions at our disposal have a volume from 25 μm^3 to 50 μm^3 with a voxel size of 25 nm. Examples of 3D reconstructions of real microstructures with volumes of 17.5 μm^3 are shown in Fig. 1 and Fig. 2.
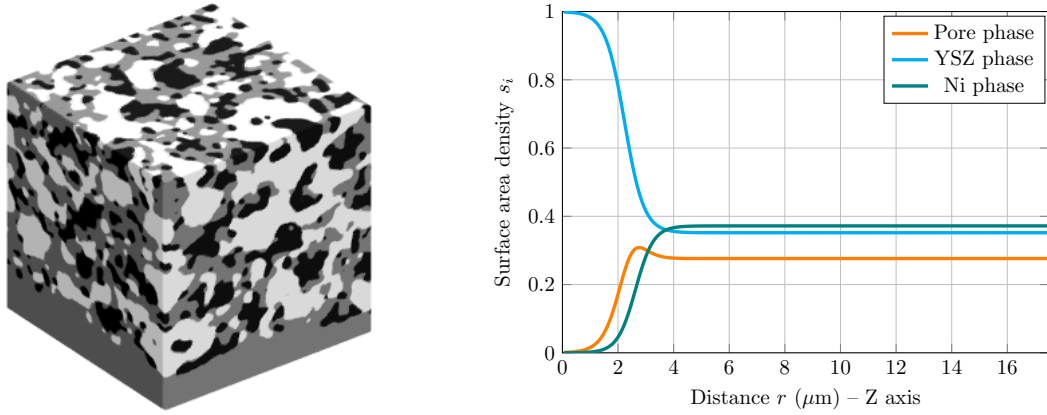

Figure 1: (Left) 3D reconstruction of a real microstructure before use. Cube of 17.5 μm side (350^3 voxels). The porous phase is in black, the ceramic phase in grey and the metallic phase in white. (Right) Evolution of the phase surface area density associated with each phase along the Z-axis.

Figure 2: (Left) 3D reconstruction of a real microstructure after 1000 h of use. Cube of 17.5 μm side (350^3 voxels). The porous phase is in black, the ceramic phase in grey and the metallic phase in white. (Right) Evolution of the phase surface area density associated with each phase along the Z-axis.
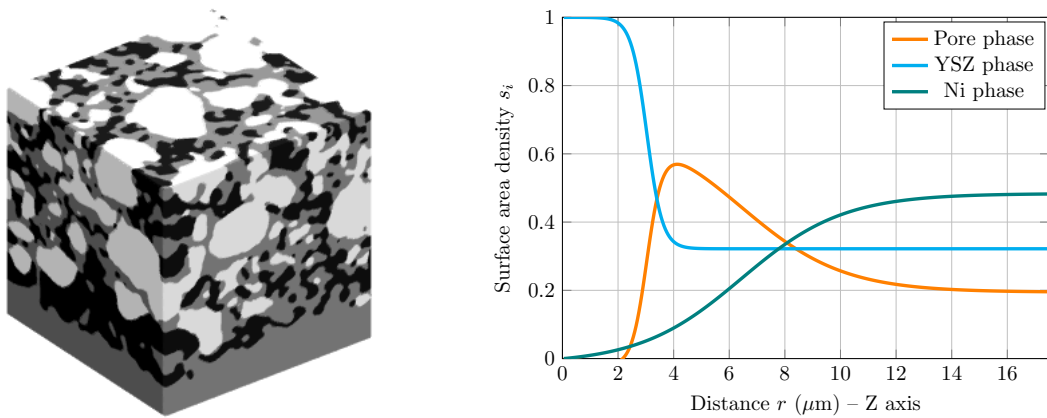
2.2 Image characterization

The microstructure of an electrode can in principle be completely characterized by a set of properties that are directly measurable on the 3D volume. The computation of these properties and their meaning has already been described in detail in the literature, as for instance in articles [9], [11] and [8].

- The volume fraction ε_i represents the ratio of volume occupied by a phase i to the total volume of the microstructure.

- The specific surface area S_p^i that represents the normalized surface area of phase i.

- The interfacial specific surface area $S_p^{i,j}$ between two phases i and j allows to completely characterize the specific surface areas S_p^k for any phase k by linear combination.

- The density of Triple Phase Boundary length or TPBl ξ_{TPBl} is calculated by identifying each voxel edges at the triple contacts.

Throughout the rest of this article, the porous, YSZ and Nickel phases are referred to the label 0, 1 and 2 respectively. Table 1 shows some properties measured on the microstructure reconstructions in Fig. 1 and Fig. 2. The phase surface area density s_i is defined on each slice of the microstructure along the Z-axis, which corresponds to the vertical axis on Fig. 1 and Fig. 2, and is the ratio of the surface area of phase i to the total area of the slice. Hence, we have the following result

$$\varepsilon_i = \frac{1}{l_z} \int_0^{l_z} s_i(z) dz \tag{1}$$

where l_z is the length of the domain W along the Z-axis.

Table 1: Properties measured on real microstructures.

Properties	Real μ-structure (Fig. 1)	Real μ-structure (Fig. 2)
ε_0	0.253	0.250
ε_1	0.424	0.439
ε_2	0.323	0.310
$S^{0,1}$	0.878 μm^{-1}	0.718 μm^{-1}
$S_p^{0,2}$	0.236 μm^{-1}	0.144 μm^{-1}
$S_p^{1,2}$	0.728 μm^{-1}	0.686 μm^{-1}
ξ_{TPBl}	1.200 μm^{-2}	0.470 μm^{-2}

Finally, to reduce the noise and fluctuations when computing $s_i(z)$, $i = \{1, 2\}$ on the microstructures, the parameters of a function g are fitted using the least squares method so that g is an approximation of s_i. The function g is defined by

$$g(z) = a + (1 - a) \times \frac{1}{1 + \exp(c \times (z - b))}. \tag{2}$$

The intention of this article is to propose a model for generating microstructures with characteristics identical to those measured on the real ones, while sharing the same global heterogeneity.

3   Stochastic model

The proposed model to simulate the phase gradients located at the interfaces of Ni-YSZ anodes is based on spatial point processes and distance maps. The process of creating a synthetic microstructure is the following.

1. A set of points $X_i \subsetneq \mathbb{R}^3$ is associated to each of the three phases. The sets X_0 and X_1 follow a Poisson point process depending only its density λ [12] while the third set X_2 follows a Neyman-Scott point process [13]. The Neyman-Scott point process requires a point density λ_p for a parent set that follows a Poisson point process. To each parent point process is attached a subset of points randomly located from a normal distribution of standard deviation σ and whose number of elements depends on a Poisson distribution of intensity λ_o (Fig. 3). Therefore, a minimum of three additional parameters is needed. Only the points of the child subsets are taken into account at the end of the process. Thus, three sets of points are generated using five parameters.

2. The three distance maps of the point sets are computed using the algorithm described in [14]. Thus, a three-phase microstructure can be built by attributing to each point of the space the set with which it has a minimum distance. Nevertheless, such a microstructure would be globally homogeneous. To introduce an heterogeneity in the microstructure, two functions $f_1(x, y, z)$ and $f_2(x, y, z)$ are used in order to modify the distance maps of the sets X_1 and X_2.

3. Finally, a two-step smoothing process described in [8] is applied. The parameter θ controlling the intensity of the smoothing allows adjusting the density of TPBl of the microstructure.

In the context of this paper, the functions f_1 and f_2 applied to the distance maps are based on sigmoids. In particular, the functions f_i, $i = \{1, 2\}$ are defined as follows.

$$f_i(z) = 1 + a_i \times \left(1 - \frac{1}{1 + \exp(c_i \times (z - b_i))}\right) \tag{3}$$

where a_i, b_i and c_i, $i = \{1, 2\}$ are parameters of shape and position.

The reason for choosing sigmoid functions is purely based on the fact that the results provided are quite satisfactory, but it would be interesting to explore other classes of functions in future work.

Fig. 4 illustrates the process of generating a microstructure with the model described above while Fig. 5 shows some examples of realizations of synthetic phase gradient microstructures. The flexibility of the model comes from its large number of parameters: five for the point processes, two functions, and one smoothing parameter. The following section details the process of fitting the input model parameters using the real reconstruction and the method validation.
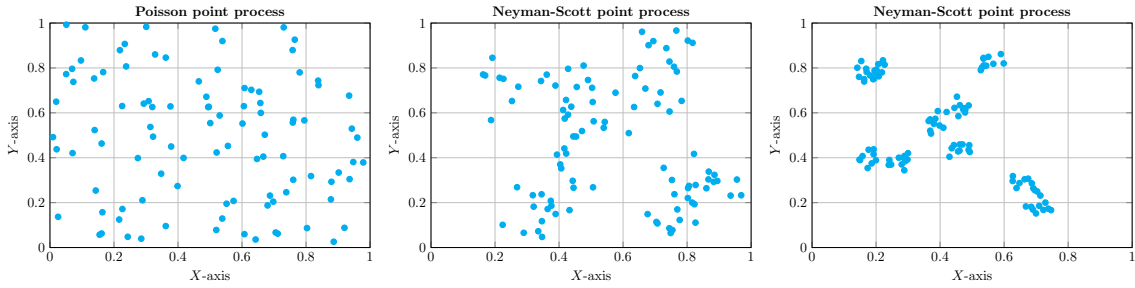

Figure 3: Example of different point processes. From left to right: Poisson point process of intensity $\lambda = 100$, Neyman-Scott point process with $\lambda_p = \lambda_o = 10$ and $\sigma = 0.075$, and Neyman-Scott point process with $\lambda_p = \lambda_o = 10$ and $\sigma = 0.025$.
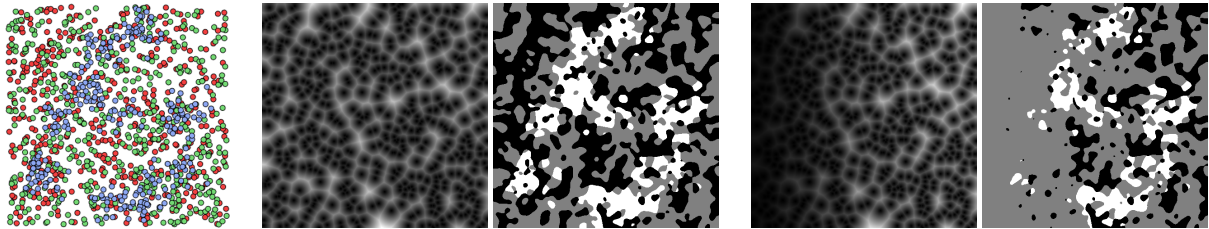

Figure 4: Illustration of the microstructure generation process (2D slice equivalent). On the left, generation of the three point sets by two Poisson processes (red and green) and a Neyman-Scott process (blue). In the center, distance map of the ceramic (gray) phase and resulting microstructure. On the right, application of a sigmoid function to the distance map of the ceramic (gray) phase and resulting microstructure.
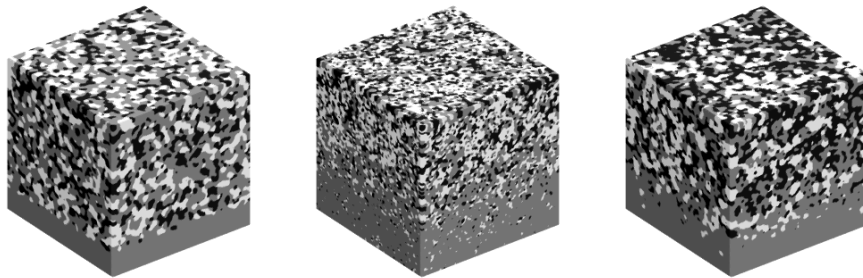

Figure 5: Example of different realizations of synthetic microstructures with phase gradient from the proposed model on a domain $W = [0; 350]^3$.

4

4 Model fitting and validation

4.1 Cost function definition

To fit the model on the real data, a cost function on $\mathbb{R}^{12}$ must be defined since the model depends on 12 parameters. Indeed, as mentioned earlier, the model depends on five parameters for the point processes, six for the two functions acting on the distance maps and defined by (3), and one smoothing parameter. The proposed cost function is defined as follows.

$$F(\omega) = \sum_{i=1}^{2} \Delta \left(\|s_i(z)\|_{\mathcal{L}_2} \right) + \sum_{0 \leq i < j \leq 2} \Delta(S^{i,j}) + \Delta(\xi_{\text{TPBl}}) \tag{4}$$

where $\omega \in \mathbb{R}^{12}$ is a set of model parameters, $\Delta \left(\|s_i(z)\|_{\mathcal{L}_2} \right)$ is the relative error on the $\mathcal{L}_2$ norm of the phase surface area density function $s_i(z)$ of phase i, $\Delta(S^{i,j})$ is the relative error on the interfacial specific surface area between phases i and j and $\Delta(\xi_{\text{TPBl}})$ the relative error of TPBl density. The fitting process then consists of applying the CMA-ES algorithm [15] to the cost function defined by equation (4) above.

4.2 Fitting process validation

In order to validate the method, it is necessary to apply the process to a synthetic structure generated by the model using a set of known parameters ω_0 and compare it to the set of parameters $\widehat{\omega}_0$ obtained after minimizing the cost function.

Table 2: Comparison of the values used to generate a synthetic microstructure with those returned by the fitting process.

Parameters	Original values (ω_0)	Fitted values ($\widehat{\omega}_0$)	Error
λ_0	12.67 μm^{-3}	12.24 μm^{-3}	-3%
λ_1	15.70 μm^{-3}	14.98 μm^{-3}	-5%
λ_p	0.95 μm^{-3}	0.98 μm^{-3}	4%
λ_o	19.51	18.9	-3%
σ	0.182 μm	0.189 μm	4%
θ	3.31	3.25	-2%
a_1	-0.61	-0.59	3%
b_1	0.16	0.16	-1%
c_1	-55.44	-57.24	3%
a_2	2.04	1.96	-4%
b_2	0.22	0.21	-4%
c_2	-42.56	-39.84	-6%

Table 2 and Fig. 6 illustrate the result obtained at the end of the fitting process. It can be seen that the relative error on each of the parameters of the model is relatively small, in the order of 3% to 4% on average. The parameters λ_0 and λ_1 correspond to the intensity of the two Poisson point processes of the two first set of points. The parameters λ_p (parents), λ_o (offspring) and σ control the Neyman-Scott point process. The parameter θ is the smoothing parameter and a_i, b_i and c_i define the function f_i as described in equation (3) for $i \in \{1, 2\}$.

Thus, Fig. 6 shows that the phase surface area density of each of the phases is very well approximated. The fitting process being validated, the following section presents the results obtained by applying it to real microstructures.

4.3 Model validation

The optimization process is performed on the two microstructures shown in Fig. 1 and Fig. 2 and the results are presented on Fig. 7 and Fig. 8. The fit on the YSZ phase is always good, whatever the microstructure considered. On the other hand, the fit on the Ni phase and the pore phase are more challenging.

Nevertheless, Table 3 and Table 4 show that the properties of the synthetic microstructures generated by the model after optimization are very close to those of the real microstructures. The higher errors on the interfacial specific surface areas are due to the simplicity of the model which, despite the use of a Neyman-Scott type aggregated point process, is not yet able to reproduce perfectly the Ni phase coarsening.

Fig. 6, 7 and 8 also show that the more locally homogeneous the microstructure, the better the results. This last hypothesis has been tested and confirmed on synthetic microstructures, in particular those shown in Fig. 5.
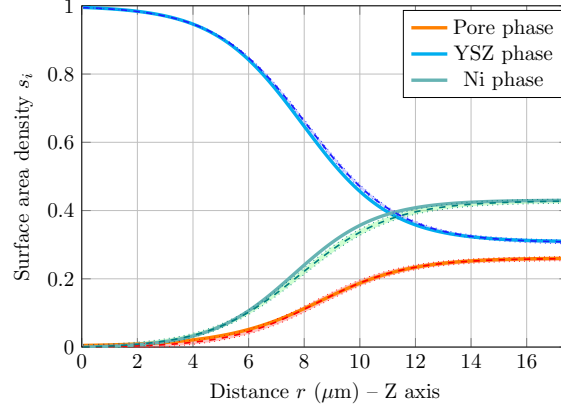
Figure 6: Comparison of phase surface area density for the original synthetic microstructure (solid lines) and the synthetic microstructure obtained after optimization of the cost function (dashed lines). The area around those corresponds to the standard deviation. The corresponding microstructure is shown on the right in Fig. 5.

Table 3: Comparison of the properties of the real microstructure and the synthetic microstructure in Fig. 7.

Properties	Real values	Simulation	Error
ε_0	0.253	0.250	-1%
ε_1	0.424	0.433	2%
ε_2	0.323	0.317	-1.8%
$S^{0,1}$	0.878 μm^{-1}	0.890 μm^{-1}	1.4%
$S_p^{0,2}$	0.236 μm^{-1}	0.230 μm^{-1}	-2.5%
$S_p^{1,2}$	0.728 μm^{-1}	0.686 μm^{-1}	-5.7%
ξ_{TPBl}	1.200 μm^{-2}	1.162 μm^{-2}	-3.3%

Table 4: Comparison of the properties of the real microstructure and the synthetic microstructure in Fig. 8.

Properties	Real values	Simulation	Error
ε_0	0.250	0.248	-0.8%
ε_1	0.439	0.439	0%
ε_2	0.310	0.312	0.5%
$S_p^{0,1}$	0.718 μm^{-1}	0.842 μm^{-1}	17%
$S_p^{0,2}$	0.144 μm^{-1}	0.138 μm^{-1}	-4.2%
$S_p^{1,2}$	0.470 μm^{-1}	0.442 μm^{-1}	-5.9%
ξ_{TPBl}	0.640 μm^{-2}	0.640 μm^{-2}	0%

5 Conclusion

An original 3D stochastic model allowing to simulate real microstructures with strong gradient and global heterogeneity has been proposed. The flexibility of the model allows to generate microstructures of various local homogeneity, and with very diverse characteristics. Thus, it was possible to fit the model on real microstructure reconstructions with rather satisfactory results, both in terms of phase surface area density curves and global characteristics of the microstructure.

It became clear that the greater the local homogeneity, the better the results. Nevertheless, the primary objective of this work, namely the simulation of phase gradient globally heterogeneous microstructure has been achieved.

In the future, it would be worthwhile to extend the model to generate microstructures even closer to those shown in Fig. 2, where the Nickel phase forms very large clusters.
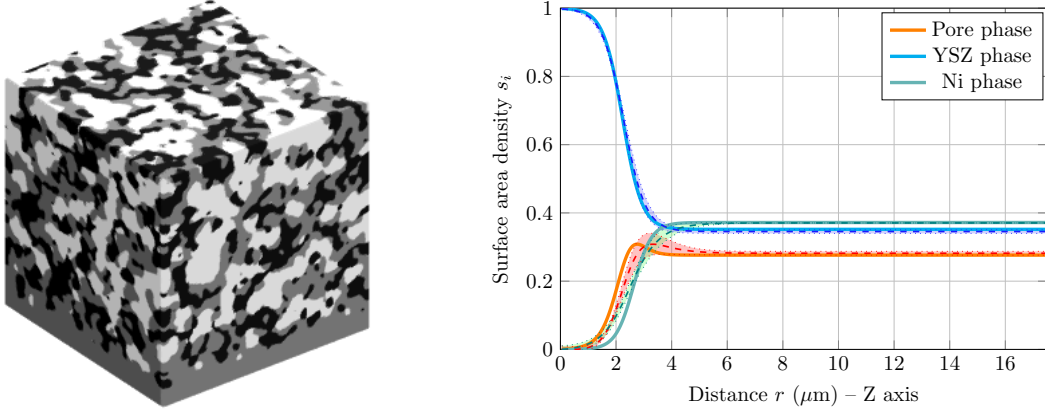
Figure 7: (Left) 3D reconstruction of a synthetic microstructure with the same properties as the microstructure in Fig. 1. (Right) Evolution of the phase surface area density. Real data (solid lines) and simulations (dashed lines). The area around those corresponds to the standard deviation. Average over a set of 8 realizations.
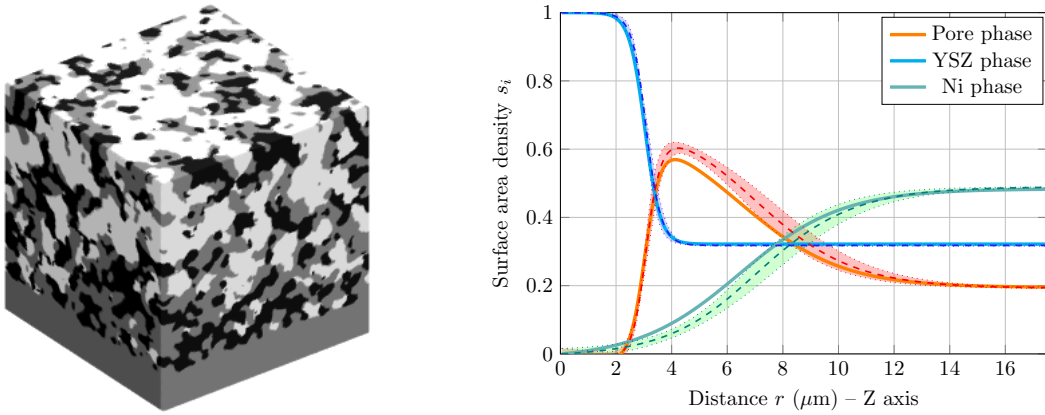

Figure 8: (Left) 3D reconstruction of a synthetic microstructure with the same properties as the microstructure in Fig. 2. (Right) Evolution of the phase surface area density. Real data (solid lines) and simulations (dashed lines). The area around those corresponds to the standard deviation. Average over a set of 8 realizations.

Acknowledgment

References

[1] J. Kong, K. Sun, D. Zhou, N. Zhang, J. Mu and J. Qiao, "Ni–YSZ gradient anodes for anode-supported SOFCs," Journal of Power Sources, vol. 166(2), 2007, pp. 337–342.

[2] M. Hubert, J. Laurencin, P. Cloetens, B. Morel, D. Montinaro, and F. Lefebvre-Joud, "Impact of Nickel Agglomeration on Solid Oxide Cell Operated in Fuel Cell and Electrolysis Modes," Journal of Power Sources, Elsevier, 2018.

[3] A. Zekri, K. Herbrig, M. Knipper, J. Parisi, T. and Plaggenborg, "Nickel Depletion and Agglomeration in SOFC Anodes During Long-Term Operation," Fuel Cells, 2017, vol. 17, pp. 359–366.

[4] D. Westhoff, I. Manke and V. Schmidt, "Generation of virtual lithium-ion battery electrode microstructures based on spatial stochastic modeling," Computational Materials Science, vol. 151, 2018, pp. 53–64.

[5] H. Moussaoui, J. Debayle, Y. Gavet, P. Cloetens and J. Laurencin, "Particle-based model for functional and diffusion layers of solid oxide cells electrodes," Powder Technology, Elsevier, vol. 367, 2020, 67–81.

[6] H. Moussaoui, J. Laurencin, Y. Gavet, G. Delette, M. Hubert, P. Cloetens, T. Le Bihan and J. Debayle, "Stochastic geometrical modeling of solid oxide cells electrodes validated on 3D reconstructions," Computational Materials Science, vol. 143, 2018, 262–276.

[7] B. Prifling, M. Ademmer, F. Single, O. Benevolenski, A. Hilger, M. Osenberg, I. Manke and V. Schmidt, "Stochastic 3D microstructure modeling of anodes in lithium-ion batteries with a particular focus on local heterogeneity," Computational Materials Science, vol. 192, 2021, 110354.

[8] M. Neumann, J. Stanek, O. M. Pecho, L. Holzer, V. Benes and V. Schmidt, "Stochastic 3D modeling of complex three-phase microstructures in SOFC-electrodes with completely connected phases," Computational Materials Science, vol. 118, 2016, pp. 353–364.

[9] J. Laurencin, R. Quey, G. Delette, H. Suhonen, P. Cloetens and P. Bleuet, "Characterisation of Solid Oxide Fuel Cell Ni–8YSZ substrate by synchrotron X-ray nano-tomography: from 3D reconstruction to microstructure quantification," Journal of Power Sources, vol. 198, 2012, pp. 182–189.

[10] J. Villanova, J. Laurencin, P. Cloetens, P. Bleuet, G. Delette, H. Suhonen and F. Usseglio-Viretta, "3D phase mapping of solid oxide fuel cell YSZ/Ni cermet at the nanoscale by holographic X-ray nanotomography," Journal of Power Sources, vol. 243, 2013, pp. 841–849.

[11] F. Usseglio-Viretta, J. Laurencin, G. Delette, J. Villanova, P. Cloetens and D. Leguillon, "Quantitative microstructure characterization of a Ni–YSZ bi-layer coupled with simulated electrode polarisation," Journal of Power Sources, vol. 256, 2014, pp. 394–403.

[12] J.F.C. Kingman, "Poisson Processes," Oxford University Press, Oxford, vol. 3, 1992.

[13] J. Neyman and E. L. Scott. "Statistical Approach to Problems of Cosmology," Journal of the Royal Statistical Society. Series B (Methodological), vol. 20, no. 1, [Royal Statistical Society, Wiley], 1958, pp. 1–43.

[14] P.F. Felzenszwalb and D.P. Huttenlocher, "Distance Transforms of Sampled Functions," Theory of Computing, vol. 8, 2012, pp. 415–428.

[15] A. Anne and H. Nikolaus, "A Restart CMA Evolution Strategy With Increasing Population Size," Proc. IEEE Congress Evolutionary Computation, vol. 2, 2005, pp. 1769–1776.